Phase diagram and structure of colloid-polymer mixtures confined between walls

R. L. C. Vink,[1,2] A. De Virgiliis,[1] J. Horbach,[1] and K. Binder[1]
[1]*Institut für Physik, Johannes-Gutenberg-Universität Mainz, Staudinger Weg 7, D-55099 Mainz, Germany*
[2]*Institut für Theoretische Physik II, Heinrich-Heine-Universität Düsseldorf, Universitätsstraße 1, D-40225 Düsseldorf, Germany*
(Received 30 June 2006; published 8 September 2006)

The influence of confinement, due to flat parallel structureless walls, on phase separation in colloid-polymer mixtures, is investigated by means of grand-canonical Monte Carlo simulations. Ultrathin films, with thicknesses between $D=3-10$ colloid diameters, are studied. The Asakura-Oosawa model [J. Chem. Phys. **22**, 1255 (1954)] is used to describe the particle interactions. To simulate efficiently, a "cluster move" [J. Chem. Phys. **121**, 3253 (2004)] is used in conjunction with successive umbrella sampling [J. Chem. Phys. **120**, 10925 (2004)]. These techniques, when combined with finite size scaling, enable an accurate determination of the unmixing binodal. Our results show that the critical behavior of the confined mixture is described by "effective" critical exponents, which gradually develop from values near those of the two-dimensional Ising model, to those of the three-dimensional Ising model, as D increases. The scaling predictions of and Fisher and Nakanishi [J. Chem. Phys. **75**, 5875 (1981)] for the shift of the critical point are compatible with our simulation results. Surprisingly, however, the colloid packing fraction at criticality approaches its bulk ($D\rightarrow\infty$) value nonmonotonically, as D is increased. Far from the critical point, our results are compatible with the simple Kelvin equation, implying a shift of order $1/D$ in the coexistence colloid chemical potential. We also present density profiles and pair distribution functions for a number of state points on the binodal, and the influence of the colloid-wall interaction is studied.

DOI: 10.1103/PhysRevE.74.031601 PACS number(s): 68.08−p, 64.70.Fx, 64.60.Fr, 05.70.Jk

I. INTRODUCTION

Confinement of fluids in nanoscopic capillaries is a problem that has received long-standing attention. An interesting interplay occurs between surface effects at the confining walls, such as wetting or drying [1–4], and finite size effects due to the finite capillary width. This interplay leads to a host of intriguing phenomena, such as capillary condensation or evaporation [5–9], and a crossover in critical behavior from three-dimensional (3D) to two-dimensional (2D) Ising character [4,5,8,10,11]. Apart from fundamental theoretical importance, understanding the structure and phase behavior of confined fluids is also a prerequisite for targeted applications in microfluidic and nanofluidic devices, which are becoming increasingly more relevant [7,12–14].

However, for fluids consisting of small molecules, complications such as the atomistic corrugation of the confining walls [15], impurity atoms at the walls, roughness of the walls due to surface steps, dislocations in the crystal structure, and so forth, may have a profound effect on the phenomena mentioned above. This is especially true when the width of the slit pore is of the order of a few nanometers, in which case a quantitative understanding becomes difficult. In this respect, colloidal dispersions, containing colloidal particles with diameters in the micrometer range, possess certain advantages. It then becomes possible to prepare slit pores which are only a few particle diameters wide, and yet have walls that are essentially flat on the size scale of the particles. In addition, interactions between colloidal particles can be well tuned [16–18]. Particularly promising systems of this kind are colloid-polymer mixtures, since both the bulk phase behavior, and the interfaces separating the colloid-rich and polymer-rich phases, can be studied experimentally in detail [19–22]. Moreover, the Asakura-Oosawa (AO) model [23,24] provides a simple theoretical framework, which seems to capture the essential features of such phase-separating systems, and is moreover well suited for computer simulations [8,25–30].

The aim of this work is to provide precise predictions for the phase diagram and the structure of the AO model confined between structureless hard walls. We consider film thicknesses ranging from $D=3$ to 10 colloid diameters. Our work complements earlier work [27,28], based on Gibbs ensemble Monte Carlo, which focused on the noncritical regime of the phase diagram. In this work, also the critical regime is considered, in order to compare to theoretical predictions for the shift in critical parameters as a function of the film thickness [5,11]. We consider a colloid-to-polymer size ratio $q=\sigma_p/\sigma_c=0.8$, with σ_c the colloid diameter and σ_p the polymer diameter of gyration, since for this particular size ratio, accurate information on the bulk and interfacial properties is available [29,30]. We also explore the effect of an additional weak repulsion between the walls and the colloids (in addition to the hard interaction already present). Understanding the combined effect of film thickness and wall-colloid interaction, is crucial in providing guidance for the interpretation of possible experiments. At this point, we are aware of only one experiment on capillary condensation of a colloid-polymer mixture (in a wedge formed by glass plates [22]), but we hope that the present study will encourage further experiments. In related previous work carried out by us, in which a film thickness $D=5$ and purely hard walls were considered, the crossover from 3D to 2D Ising critical behavior was already discussed [8].

The outline of this paper is as follows. In Sec. II we summarize the most important theoretical predictions relevant for the interpretation of our results. In Sec. III the AO model is introduced, and details on the simulation technique are provided. In Sec. IV we investigate the phase behavior

and the structural properties of the AO model as the film thickness D is varied, while Sec. V onsiders the influence of the colloid-wall interaction. Finally, in Sec. VI we summarize our main conclusions.

II. THEORETICAL BACKGROUND

We consider a system with an one-component order parameter near its critical point. Examples of such systems are fluids near their vapor-liquid critical point, magnetic systems (such as the simple Ising model), and binary mixtures (such as colloid-polymer mixtures) near their critical point of unmixing. As is well known, all these systems in 3D bulk belong to the 3D Ising universality class [31]. In particular, critical exponents such as the exponent ν (which characterizes the growth of the order parameter correlation length ξ near the critical point), or the order parameter exponent β (which characterizes the shape of the binodal between the unmixed phases in a binary mixture) have nontrivial values $\nu \approx 0.630$, $\beta \approx 0.326$ [32–34], rather than the classical mean-field values $\nu_{\mathrm{MF}}=1/2$, $\beta_{\mathrm{MF}}=1/2$.

When these systems are confined between two identical flat planar structureless walls a distance D apart, two distinct physical phenomena affecting the phase transition are expected to occur.

(i) The growth of the critical correlations in the direction perpendicular to the walls is limited by the finite thickness of the film, while critical correlations can still grow further and unlimited in the two directions parallel to the film. Therefore, a crossover from 3D critical behavior toward 2D critical behavior (for which the exponents mentioned above take the values $\nu_2=1$ and $\beta_2=1/8$, assuming 2D Ising universality [31,35]) is expected. This crossover is predicted to occur when the temperaturelike variable has approached a relative distance t from the critical point in the bulk such that $\xi \propto t^{-\nu}$ is of the same order as D, implying a crossover distance of order $t_{\mathrm{cross}} \propto D^{-1/\nu}$. This dimensional crossover in critical behavior also implies an additional enhancement of fluctuations (in lower dimensionality stronger fluctuations occur). This leads to a depression of the critical point. Consequently, one expects a shift of the critical point of the same order $t_{\mathrm{shift}} \propto D^{-1/\nu}$.

(ii) If there is no special symmetry between the coexisting phases, one must expect that there is an (energetic and/or entropic) preference of the walls for one of the coexisting phases in comparison to the other. This phenomenon is also well known to occur away from the critical point. For example, hydrophilic walls of a thin slit capillary are known to lead to "capillary condensation" of an undersaturated vapor in the capillary [36]. Of course, for hydrophobic rather than hydrophilic walls, also the opposite effect ("capillary evaporation") may occur.

Clearly, a quantitative prediction of the magnitude, and sometimes even the sign, of these effects, requires detailed knowledge of the forces between the walls and the particles confined by them. However, since phase equilibrium is always shifted due to surface corrections to the relevant thermodynamic potentials, we expect a shift in the coexistence chemical potential in the thin film, relative to its value in the bulk, of order $1/D$. This is the so-called "Kelvin equation" [4–7], which is expected to be valid away from the critical point. In contrast, the corresponding shift in the chemical potential at criticality is more subtle. This becomes most transparent for the case of an Ising magnet (or, equivalently, the lattice gas model), where in the bulk there is a symmetry between the coexisting "spin up" and "spin down" phases. However, in the thin film, this symmetry may be broken by a surface magnetic field H_1 [4,5,11,37,38]. While phase coexistence in the bulk occurs for bulk magnetic field $H=0$, coexistence in the thin film now requires a nonzero bulk field (with a sign opposite to that of the surface field H_1).

It has been shown that in the presence of the surface field, the singular part of the free energy per spin in this Ising model should scale as [4,5,11,37,38]

$$f_{\mathrm{sing}}(D,T,H,H_1) = |t|^{2-\alpha}\tilde{f}_{\pm}(D|t|^{\nu},H|t|^{-\Delta},H_1|t|^{-\Delta_1}), \qquad (1)$$

with $\alpha \approx 0.110$ [32–34] the critical exponent of the specific heat, $\Delta \approx 1.56$ [32–34] the so-called "gap exponent" which characterizes the bulk equation of state, and $\Delta_1 \approx 0.47$ [38–41] its surface analog. The scaling functions $\tilde{f}_{\pm}$, where the signs refer to the sign of t, are discussed in more detail in Refs. [5,11]. Here, we only infer from Eq. (1) that the shift in the critical temperature should read as [5]

$$t_{\mathrm{shift}} \equiv \Delta T_c/T_c(\infty) = [T_c(D,H_1) - T_c(\infty)]/T_c(\infty) = -D^{-1/\nu}X_c(H_1 D^{\Delta_1/\nu}), \qquad (2)$$

and similarly for the shift in the bulk magnetic field required to establish coexistence again

$$\Delta H_c \equiv H_c(D,H_1) = -D^{-\Delta/\nu}Y_c(H_1 D^{\Delta_1/\nu}) \overset{H_1 \to 0}{\propto} -H_1 D^{(\Delta_1-\Delta)/\nu}. \qquad (3)$$

Here, X_c and Y_c are again scaling functions, and $T_c(\infty)$ denotes the critical temperature in the bulk $(D \to \infty)$ system. Note that for small H_1, we expect that X_c tends to a constant, while Y_c becomes a linear function of its argument. This limit is relevant in the present case, since we deal with rather small film thicknesses D.

Considering now mixtures of colloids (c) and polymers (p) in the grand-canonical ensemble, chemical potentials μ_c and μ_p, of colloids and polymers, respectively, as well as temperature T and system volume V become the relevant independent thermodynamic variables. In the framework of the AO model [23,24], the dependence on temperature only enters via the fugacities $z_c=\exp(\mu_c/k_BT)$, and $z_p=\exp(\mu_p/k_BT)$. There is no other explicit temperature dependence in this model. Considering the fugacity of the polymers as a temperaturelike variable, bulk phase coexistence between a phase rich in colloids (analogous to a liquid in the liquid-vapor transition) with colloid packing fraction η_c^l, and a phase poor in colloids (analogous to the vapor) with colloid packing fraction $\eta_c^v < \eta_c^l$, occurs on the line $z_c^{\mathrm{coex}}(z_p)$. The latter is determined by the equation $\mu_c/k_BT=\mu_c^{\mathrm{coex}}(z_p)/k_BT$ in the plane of variables (z_p,z_c). The variable $\Delta\mu=\mu_c-\mu_c^{\mathrm{coex}}$ thus plays a role analogous to that of the magnetic

field H in the Ising model, and $\eta_c^l(z_p)-\eta_c^v(z_p)$ corresponds to $2m_{\rm sp}(T)$ for $H\to 0^+$, with $m_{\rm sp}(T)=-(\partial f_{\rm sing}/\partial H)_T$ the spontaneous magnetization or order parameter.

While in the Ising model there is a symmetry with respect to the sign of H, no corresponding symmetry with respect to the sign of $\Delta\mu$ occurs in colloid-polymer mixtures, of course. In the Ising model, the two branches $\pm m_{\rm sp}(T)$ of the binodal, corresponding to positive and negative fields, are equivalent; this is the particle-hole symmetry of the lattice gas. Obviously, no such symmetry exists in asymmetric mixtures. Therefore, the above identification of variables holds only to a first approximation, and for a more precise discussion of critical phenomena one needs to consider "field mixing" effects [42]. The temperaturelike variable t should then be taken parallel to the curve $z_c^{\rm coex}(z_p)$ at the point $z_c^{\rm crit}(z_p=z_p^{\rm crit})$, and the fieldlike variable H becomes a suitable linear combination of the variables $\Delta\mu$ and $z_p-z_p^{\rm crit}$ [29,30,42]. Note that the field mixing formulation of Ref. [42] does not allow for the appearance of a $|t|^{2\beta}$ term in the diameter. A more rigorous formulation, allowing for a $|t|^{2\beta}$ term, should include the pressure in the scaling fields [55].

Even more intricate becomes the identification of the variable corresponding to H_1, the local magnetic field coupling to the spins at the surface of the Ising magnet. The case $H_1=0$ physically means "neutral walls", in which case the walls prefer neither the "spin-up phase" nor the "spin-down phase" of the ferromagnet. It is not at all obvious which choice of surface interactions would correspond to such a "neutral wall", preferring neither the colloid-rich phase, nor the polymer-rich phase of our model. Of course, a completely analogous difficulty occurs in studies of capillary condensation and/or surface critical phenomena associated with the vapor-liquid critical point of ordinary fluids [43–45]. We conclude that, in general, whatever the choice for the strength and range of the particle-wall interaction, it will likely correspond to a situation $H_1\neq 0$, but we have no possibility to predict the strength (and even the sign) of H_1 beforehand. In principle, a careful analysis of order parameter profiles at the bulk critical point of a very "thick" film (which approximates a semi-infinite system with two surfaces) for various wall-particle interactions could provide insight into how to realize a situation with $H_1=0$ at criticality [38]. This, however, gives no guarantee that, for the same choice of interactions, one also has $H_1=0$ outside of the critical region.

On the other hand, if our simulations display only very small shifts of $\mu_c^{\rm coex}(z_p)/k_BT$ with decreasing film thickness, one may assume that H_1 in our model is indeed small. In this case, Eqs. (2) and (3) still hold. However, if the data indicate that this is not the case, and rather the inverse limit $H_1D^{\Delta_1/\nu}\gg 1$ is reached instead, simple power laws would again result

$$t_{\rm shift}=-D^{-1/\nu}X_c(\infty),\quad \Delta H_c=-D^{-\Delta/\nu}Y_c(\infty). \tag{4}$$

While the first power law of Eq. (4) is the same as before (only the constant of proportionality has changed), the second power law clearly implies a somewhat faster decay than found in Eq. (3). Finally, for $H_1D^{\Delta_1/\nu}\approx 1$ a crossover behavior should be detectable, but to clearly identify such behavior may be difficult. In any case, the above discussion already shows that (confined) colloid-polymer mixtures may give rise to a much more complex behavior than the simple Ising model [11], and hence their study should be rewarding.

III. MODEL AND SIMULATION TECHNIQUE

In this work, the colloids are modeled as hard spheres with diameter σ_c, while the polymers are described as spheres with diameter σ_p. The polymers may not overlap with colloids, but there is no interaction between the polymers. The choice of this model [23,24] is motivated by the fact that flexible polymers form random coils with a rather large gyration radius R_g, which may interpenetrate at very low energy cost (in particular if the solution in which the polymers are dissolved, and the colloidal particles are suspended, is close to θ-point conditions [46]). Colloids, on the other hand, can be prepared with interactions of very short range [16–18].

We specialize to a size ratio $q=\sigma_p/\sigma_c=0.8$ in the following and choose $\sigma_c=1$ as our unit of length. The polymer and colloid packing fractions are $\eta_p=\pi\sigma_p^3N_p/(6V)$ and $\eta_c=\pi\sigma_c^3N_c/(6V)$, when we have N_p polymers and N_c colloids in our system of volume V, respectively. We choose a volume in the geometry of a rectangular box of linear dimensions $L_x\times L_y\times L_z$ with $L_x=L_y=L$ and $L_z=D$, respectively. Periodic boundary conditions are applied in the x and y directions. In the remaining z direction, we place two $L\times L$ walls, at $z=0$ and $z=D$, respectively, which act as hard walls for both polymers and colloids, while in addition a repulsive step potential of height ϵ (in units of k_BT) acts on the colloids. The full colloid-wall interaction $u_{\rm cw}(h)$ thus reads as

$$u_{\rm cw}(h)=\begin{cases}\infty & \text{for } h\leqslant 0,\\ \epsilon & \text{for } 0<h<\sigma_c/2,\\ 0 & \text{otherwise},\end{cases} \tag{5}$$

with h the distance from the *surface* of the colloid to the wall. In this work, $\epsilon=0$, 0.25, 0.5, 1.0, and 2.0 are considered. Note that the case $\epsilon=0$ (purely hard walls for both colloids and polymers) and $D=5$ has already been investigated in our previous work [8]. In this case, a very strong attraction between the colloids and the walls develops due to the depletion effect [26].

Following common practice [19,29,30], we choose the so-called (dimensionless) "polymer reservoir packing fraction" $\eta_p^r\equiv\pi z_p\sigma_p^3/6$, rather than the polymer fugacity z_p, as the temperaturelike variable. As in our previous work [8,29,30], we apply a grand canonical cluster move [29], together with a very efficient reweighting scheme, successive umbrella sampling [47], in order to obtain the distribution function $P_L(\eta_c|\eta_p^r,z_c)$, defined as the probability of observing the system with colloid packing fraction η_c at "inverse temperature" η_p^r and colloid fugacity z_c. By the subscript L, we remind the reader that quite generally there will be finite size effects, and a suitable extrapolation to the limit $L\to\infty$, keeping the film thickness D fixed, may be required. While for states that are far away from phase coexistence, $P_L(\eta_c|\eta_p^r,z_c)$ is a

single-peaked function, near two-phase coexistence a double-peak structure develops. The precise location of the fugacity z_c at which two-phase coexistence occurs is obtained using the equal-weight rule [48,49]. The positions of the two peaks in $P_L(\eta_c|\eta_p^r,z_c)$ then yield estimates for the two branches, η_c^l and η_c^v, of the binodal. In addition, we also study reduced moments of $P_L(\eta_c|\eta_p^r,z_c)$ at phase coexistence, defining an analog of the order parameter of the Ising model

$$m = \eta_c - \langle \eta_c \rangle, \quad \langle \eta_c \rangle = \int_0^\infty \eta_c P_L(\eta_c|\eta_p^r,z_c) d\eta_c \tag{6}$$

and higher-order moments

$$\langle m^p \rangle = \int_0^\infty m^p P_L(\eta_c|\eta_p^r,z_c) d\eta_c. \tag{7}$$

As is well known, following the behavior of moment ratios such as

$$U_4 = \langle m^2 \rangle^2 / \langle m^4 \rangle \tag{8}$$

along the path where z_c is at phase coexistence in the (z_c, η_p^r) plane, is useful for locating the critical point of the system; this is the so-called "cumulant intersection method" [50–52]. Although it has been demonstrated recently [8,53] that a study of the full distribution $P_L(\eta_c|\eta_p^r,z_c)$ and its moments also for fugacities z_c off coexistence near criticality is useful, and can yield even more accurate information on the critical behavior, the computer time resources for such a study in the present case are very demanding, and hence not attempted here.

IV. RESULTS FOR ϵ=0.5

In this section, we present results using step height ϵ =0.5 in the colloid-wall interaction of Eq. (5). We ultimately aim to test the Fisher-Nakanishi scaling predictions [5] for the shift in the critical point parameters. To this end, the location of the critical point as function of the film thickness D, the binodal, and the behavior of the critical colloid packing fraction are investigated first.

A. Critical point

We aim to locate the critical value of η_p^r, for a number of thicknesses D. To this end, the cumulant ratio U_4, see Eq. (8), was measured as function of η_p^r using several lateral dimensions L. The results are shown in Figs. 1 and 2 for D =5 and D=10, respectively. We found that for $D \leqslant 10$, simulation data of meaningful accuracy could still be generated, although for D=10 there is the need to choose the lateral linear dimension L as large as L=40. From the cumulant intersection points, $\eta_{p,\mathrm{cr}}^r$ is obtained. The "effective" correlation length exponent ν_{eff} is obtained from the L dependence of the cumulant slope Y_1 evaluated at the intersection point. One expects that $Y_1 \propto L^{1/\nu_{\mathrm{eff}}}$; the insets in Figs. 1 and 2 show that our simulation estimates of Y_1 are indeed compatible with this relation. Additional simulations were performed for thicknesses D=3 and D=7.5; the resulting estimates of $\eta_{p,\mathrm{cr}}^r$

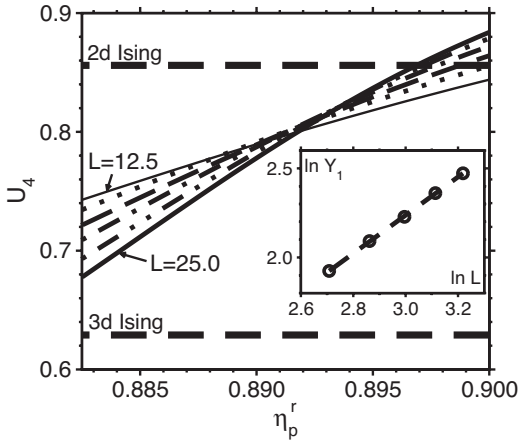

FIG. 1. Moment ratio U_4 for a film of thickness D=5 plotted versus the polymer reservoir packing fraction η_p^r and several choices of the lateral dimension L=12.5, 15.0, 17.5, 20.0, 22.5, and 25.0. The intersection point yields an estimate for the critical "inverse temperature" $\eta_{p,\mathrm{cr}}^r$=0.892. The inset shows a log-log plot of the cumulant slope Y_1 versus the linear dimension L. The straight line yields the exponent $1/\nu_{\mathrm{eff}}$, from which we deduce ν_{eff}=0.933.

and ν_{eff}, as well as the cumulant value U_4^* at the critical point, and the corresponding coexistence colloid chemical potential, are collected in Table I. From these data, it is clear that, by increasing the film thickness D, a gradual crossover in the effective critical behavior from 2D Ising toward 3D Ising universality occurs. While for D=3, ν_{eff} is very close to the exact value ν=1 of the 2D Ising model, and similarly for the corresponding cumulant value U_4^* (for the 2D Ising model, the very precise estimate U_4^*=0.856 was obtained [54]), with increasing D a clear shift toward 3D Ising values is observed.

Of course, the smooth decrease of these "effective" values can only be taken as a very rough description of the theoretically expected crossover scaling scenario [8–11]. For the

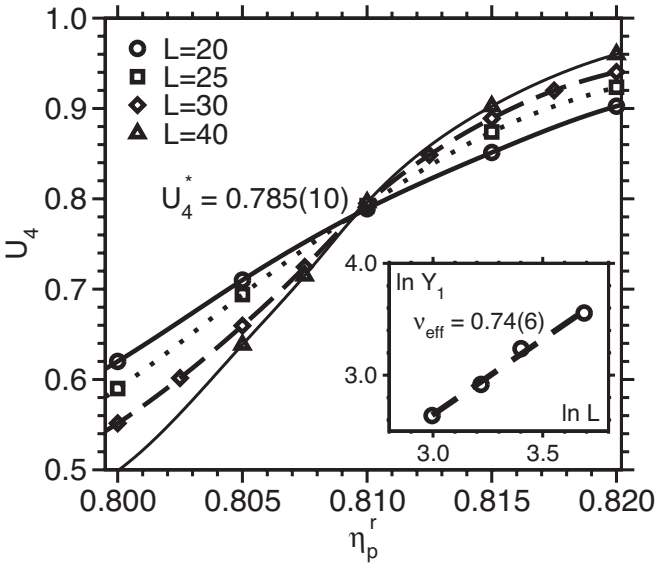

FIG. 2. Same as Fig. 1, but for film thickness D=10, yielding the estimates $\eta_{p,\mathrm{cr}}^r$=0.810 and ν_{eff}=0.74.

TABLE I. Critical parameters of the AO model for different film thicknesses D, compared to the corresponding 2D and 3D bulk values. Note that the simulation data reported in this table were obtained using ϵ=0.5 as step height in the colloid wall interaction of Eq. (5).

D	ν	U_4^*	$\eta_{p,cr}^r$	$\mu_{c,cr}^{coex}(D)$	δ^*
2D bulk	1	0.856			
3.0	0.955(5)	0.84(1)	1.055(5)	4.39(2)	0.139(1)
5.0	0.933(3)	0.81(1)	0.892(4)	3.715(15)	0.142(1)
7.5	0.805(5)	0.80(1)	0.834(4)	3.43(2)	0.143(1)
10.0	0.74(6)	0.785(10)	0.810(5)	3.307(7)	0.141(1)
3D bulk	0.630	0.629	0.766	3.063	0.134

case of D=5 and hard-wall boundary conditions, a more elaborate analysis is presented in Ref. [8]. While in this case the cumulant slopes yield the same "effective" exponent $\nu_{\text{eff}} \approx 0.933$ as found here for D=5 [8], the more elaborate analysis in fact revealed [8] that the asymptotic critical behavior is in reality described *precisely* by 2D critical exponents, but this can be seen only in a very narrow region around the critical point. Analyzing any such critical quantity on a log-log plot, one typically finds a systematic curvature: the slope of the curve approaches the 2D value for very small $|t|$ and then very gradually bends over in the direction towards the 3D value (the latter is not really observed because the crossover is not yet complete as $|t|$ becomes so large that one leaves the critical region) [8]. Since a thorough analysis of crossover scaling requires an enormous investment of computer resources, we have refrained from doing so, since there is no reason to expect any significant surprises.

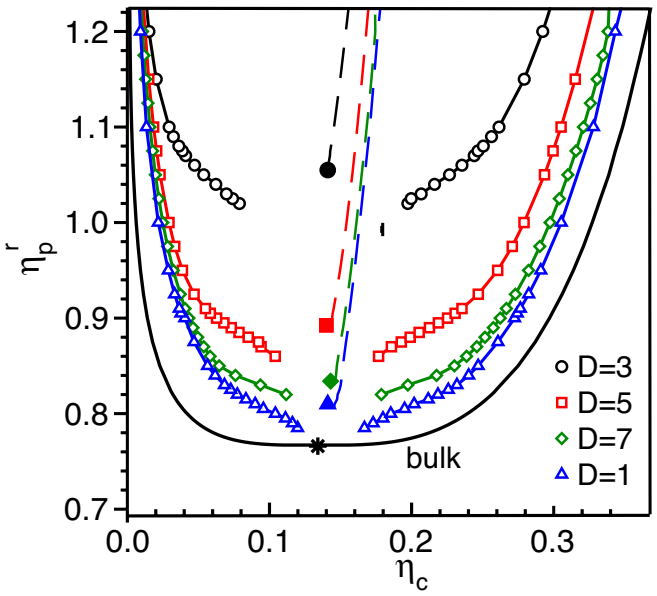

FIG. 3. (Color online) Binodals of the AO model with q=0.8 in bulk (full curve without data points) and in confinement by parallel hard walls, to which a repulsive potential on the colloids with strength ϵ=0.5 was added [see Eq. (5)]. Circles denote data for D=3, L=18; squares for D=5, L=20; diamonds for D=7.5, L=30; and triangles for D=10, L=30. The dotted lines denote the estimated coexistence diameters.

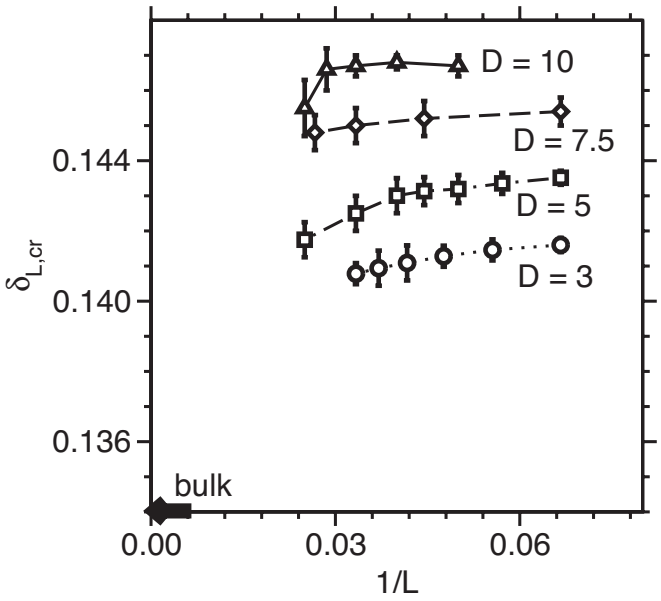

FIG. 4. Finite size coexistence diameters $\delta_{L,cr}$ as function of $1/L$, for various choices of D as indicated. The arrow marks the diameter at the critical point in the thermodynamic limit of the bulk system, i.e., in the absence of walls, and was taken from Ref. [30].

B. Binodal and coexistence diameter

Next, we consider the binodal. Figure 3 shows some of our "raw" data for the binodals in confinement, together with our estimates of the corresponding coexistence diameters (broken lines). By "raw" we mean that no finite size scaling analysis was performed on the data. The coexistence diameter δ is defined as the average of the coexisting phase densities

$$\delta = (\eta_c^l + \eta_c^v)/2, \tag{9}$$

where, as before, η_c^v and η_c^l represent the coexistence colloid packing fractions on the vapor and liquid branches of the binodal, respectively. The diameters terminate at the critical value of η_p^r, for which we used the estimates listed in Table I. Since the data were obtained for finite $L \leqslant 30$, the two branches of the binodal do not merge at the critical point, but rather extend beyond it, bending over into the one-phase region. This effect of "finite size tails" or "rounding" of the order parameter into the disordered region of the phase diagram is well known from simulations of the Ising model [50–52]. It is due to the fact that the order parameter distribution is clearly double peaked right at criticality and also in the one-phase region, if the lateral linear dimension L does not yet exceed the correlation length [50–52]. The exception in Fig. 3 is the full curve, which represents the binodal of the 3D bulk AO model. This curve was obtained using the finite size scaling approach of Ref. [53], and, on the scale of Fig. 3, should rather precisely reflect the true thermodynamic limit form $L \to \infty$ of the bulk binodal.

In order to more accurately determine the colloid packing fraction at the critical point $\eta_{c,\mathrm{cr}}$, we have examined the L dependence of $\delta_{L,\mathrm{cr}}$, defined as the value of the coexistence diameter δ, given by Eq. (9), as obtained in a finite system of lateral dimension L, at the critical value of η_p^r. The result is shown in Fig. 4, where $\delta_{L,\mathrm{cr}}$ is plotted as function of $1/L$, using for $\eta_{p,\mathrm{cr}}^r$ the values listed in Table I. The data display significant scatter, but rather intriguing behavior is revealed nevertheless. By increasing the film thickness D, also $\delta_{L,\mathrm{cr}}$ increases, away from the bulk value (arrow in Fig. 4), although in the limit $D\to\infty$ precisely this bulk value should be recovered again. A possible explanation for this nonmonotonic behavior with D, may be found in the precise critical behavior of the coexistence diameter in the thermodynamic limit. The critical behavior of δ in the limit $L\to\infty$ is rather intricate, and governed by several competing singular terms [55]

$$\delta = \eta_{c,\mathrm{cr}}(1 + A_{2\beta}t^{2\beta} + A_{1-\alpha}t^{1-\alpha} + A_1 t + \cdots), \qquad (10)$$

with relative distance from the critical point $t \equiv \eta_p^r/\eta_{p,\mathrm{cr}}^r - 1$, (nonuniversal) amplitudes A_i, and $\eta_{c,\mathrm{cr}}$ the colloid packing fraction at the critical point. Note that in 2D, the first singular term has a much smaller exponent ($2\beta = 1/4$), but also the amplitude $A_{2\beta}$ may be very small compared to the amplitudes of the other terms. The next order term may involve a logarithmic correction [56]; recall that $\alpha = 0$ in the 2D Ising model implies a logarithmic divergence of the specific heat. It is expected that in a finite system, the singular terms $t^{2\beta} \propto \xi^{-2\beta/\nu}$ and $t^{1-\alpha} \propto \xi^{-(1-\alpha)/\nu}$, crossover to correction terms, with ξ ultimately replaced by L. Hence, we expect for the quantity $\delta_{L,\mathrm{cr}}$ in Fig. 4 the scaling form

$$\delta_{L,\mathrm{cr}} = \eta_{c,\mathrm{cr}}(D)[1 + \hat{A}_{2\beta}(D/L)L^{-2\beta/\nu} + \hat{A}_{1-\alpha}(D/L)L^{-(1-\alpha)/\nu} + \hat{A}_1(D/L)L^{-1/\nu} + \cdots]. \qquad (11)$$

Here, we have assumed that the amplitudes $\hat{A}_i$ are functions of the aspect ratio D/L; such a dependence can be motivated by finite size scaling arguments [10,11]. In view of the rather large error bars in $\delta_{L,\mathrm{cr}}$ in Fig. 4, and the complicated structure of Eq. (11), we feel that an accurate extrapolation to obtain $\eta_{c,\mathrm{cr}}(D)$ is not possible. Similarly, already in Ref. [8], it was pointed out that a reliable estimate of the critical behavior of the diameter in confinement from simulation data is not yet feasible. Hence, the only tentative conclusion we can draw from Fig. 4 is that presumably the dependence of $\eta_{c,\mathrm{cr}}(D)$ on D is nonmonotonic: $\eta_{c,\mathrm{cr}}(D)$ for small D does not differ much from $\eta_{c,\mathrm{cr}}(\infty)$, but with increasing D the difference increases first, reaches a maximum, and then decreases again. Such behavior could stem from competing signs of some of the amplitudes in Eqs. (10) and (11).

For completeness, Fig. 5 shows $\delta^* \equiv \lim_{L\to\infty}\delta_{L,\mathrm{cr}}$ as function of D^{-1}, where δ^* was obtained by linearly extrapolating the data for $\delta_{L,\mathrm{cr}}$ of Fig. 4 in the variable $1/L$. The resulting estimates of δ^* have also been collected in Table I, and reflect our best possible estimates of the critical colloid packing packing fraction $\eta_{c,\mathrm{cr}}$ in the thermodynamic limit [recall that Eq. (10) for the diameter reduces to $\eta_{c,\mathrm{cr}} = \delta^*$ at the critical point $t\to 0$]. It is plausible from these data that the variation of δ^* with D^{-1} is indeed nonmonotonic. However, the large error bars in δ^*, resulting from the uncertainty in the extrapolation of $\delta_{L,\mathrm{cr}}$ to $L\to\infty$, prevent us from making any quantitative statements. In contrast, at values of η_p^r that are far from the critical point for all choices of D considered here, such as $\eta_p^r = 1.1$, the L dependence in the diameter can

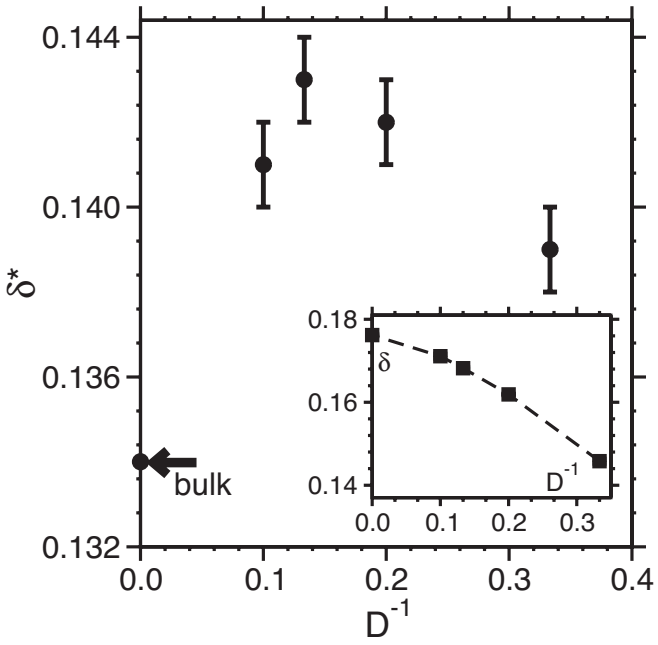

FIG. 5. Variation of the diameter at the critical point $\delta^* = \lim_{L\to\infty}\delta_{L,\mathrm{cr}}$ as function of D^{-1}. The inset shows the diameter δ away from the critical point, choosing $\eta_p^r = 1.1$, as function of D^{-1}.

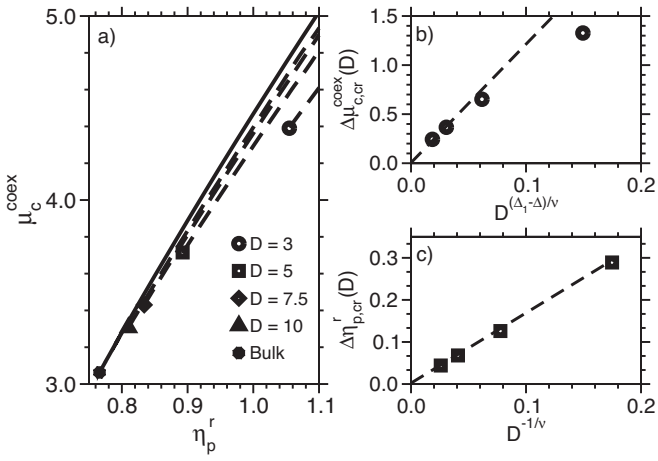

FIG. 6. (a) Binodals of the AO model with $q = 0.8$ in the so-called grand-canonical representation, choosing the coexistence chemical potential of the colloids μ_c^{coex} and η_p^r as variables. Shown is the bulk binodal (full curve), and the binodal in confinement for several film thicknesses D (broken curves). The symbols mark the corresponding critical points. (b) Shift of the critical coexistence colloid chemical potential, given by Eq. (13), as function of $D^{(\Delta_1-\Delta)/\nu}$. (c) Shift of the critical polymer reservoir packing fraction, given by Eq. (12), as a function of $D^{-1/\nu}$. Linear straight line fits through the origin in (b) and (c) confirm that the data are compatible with the theoretical Fisher-Nakanishi predictions [5].

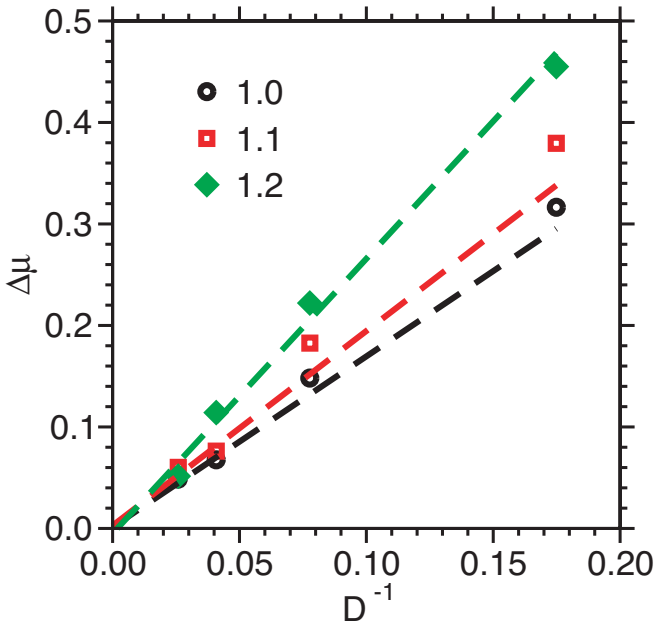

FIG. 7. (Color online) Test of the Kelvin equation. Shown is the chemical potential difference, given by Eq. (14), as function of the inverse film thickness. Three values of η_p^r, chosen well above the critical values $\eta_{p,\mathrm{cr}}^r(D)$, are included. Broken straight lines show that the data are compatible with the Kelvin equation.

safely be neglected. In this case, the variation with D^{-1} is clearly monotonic, and approximately linear for small D^{-1}, see the inset of Fig. 5.

C. Fisher-Nakanishi scaling and Kelvin equation

Next, we consider the Fisher-Nakanishi scaling predictions, essentially the main result of this paper. Recall from the discussion in Sec. II, that the Fisher-Nakanishi scaling predictions pertain to the shift in the critical point parameters. More precisely, for the shift in the critical "inverse temperature" as function of the film thickness D, one expects that

$$\Delta \eta_{p,\mathrm{cr}}^r(D) \equiv \eta_{p,\mathrm{cr}}^r(D) - \eta_{p,\mathrm{cr}}^r(\infty) \propto D^{-1/\nu}, \qquad (12)$$

with ν the correlation length critical exponent of the 3D Ising model, $\eta_{p,\mathrm{cr}}^r(D)$ the critical value of η_p^r in the confined system of thickness D, and $\eta_{p,\mathrm{cr}}^r(\infty)$ the critical value of η_p^r in the bulk $(D \to \infty)$ system. The second scaling prediction of Fisher and Nakanishi pertains to the shift in the coexistence chemical potential of the colloids at criticality, as function of the film thickness D. It is expected that

$$\Delta \mu_{c,\mathrm{cr}}^{\mathrm{coex}}(D) \equiv \mu_{c,\mathrm{cr}}^{\mathrm{coex}}(D) - \mu_{c,\mathrm{cr}}^{\mathrm{coex}}(\infty) \propto D^{(\Delta_1-\Delta)/\nu}, \qquad (13)$$

with Δ and Δ_1 the gap exponents introduced in Sec. II, ν again the correlation length exponent of the 3D Ising model, $\mu_{c,\mathrm{cr}}^{\mathrm{coex}}(D)$ the coexistence chemical potential of the colloids at criticality in the confined system, and $\mu_{c,\mathrm{cr}}^{\mathrm{coex}}(\infty)$ the coexistence chemical potential of the colloids at criticality in the bulk system. Our results have been collected in Fig. 6. The left panel shows the coexistence chemical potential μ_c^{coex} of

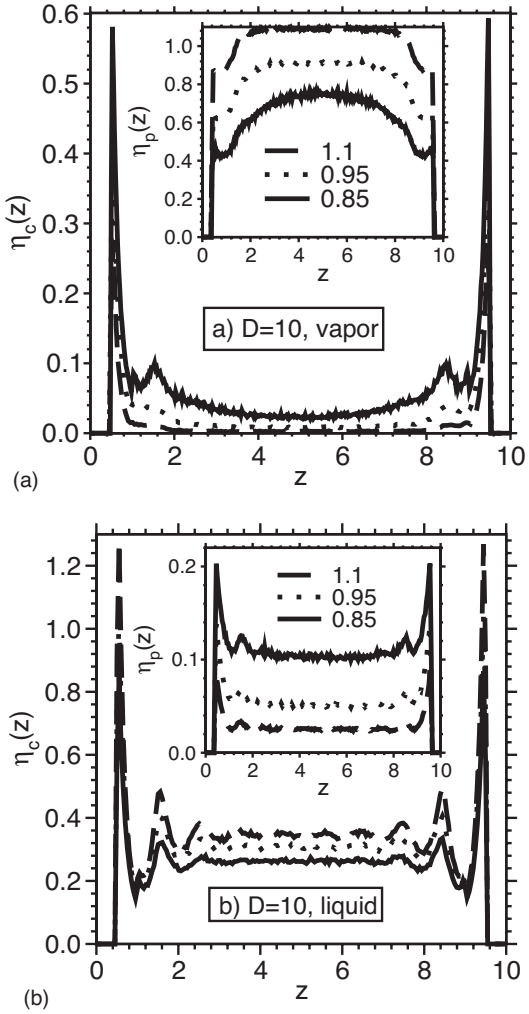

FIG. 8. Colloid density profiles for film thickness $D=10$ and lateral dimension $L=30$. Profiles were obtained for three different values of η_p^r, as indicated, chosen to be well away from the critical point. Shown are profiles measured on the vapor branch of the binodal (a) and on the liquid branch (b). The insets show the corresponding polymer density profiles.

the colloids as a function of η_p^r, for several values of the film thickness D. We remind the reader that the coexistence chemical potential of the colloids follows from the equal-weight-rule [48,49]. The shift in the coexistence chemical potential of the colloids at criticality, see Eq. (13), is plotted in Fig. 6(b), as function of $D^{(\Delta_1-\Delta)/\nu}$. Here, the chemical potential shifts were simply read-off from Fig. 6(a); the corresponding values have also been collected in Table I for completeness. The shift in the critical "inverse temperature," see Eq. (12), is plotted in Fig. 6(c), as function of $D^{-1/\nu}$, where for the critical values of η_p^r, the estimates of Table I were used. In Figs. 6(b) and 6(c), the known values of the exponents were used, as quoted previously. Validity of the Fisher-Nakanishi relations implies that the data collapse onto straight lines through the origin. Of course, data for small D, such as $D=3$ and $D=5$, need not follow these relations, because the Fisher-Nakanishi predictions are valid only for *asymptotically* large D. For small D, corrections to finite size

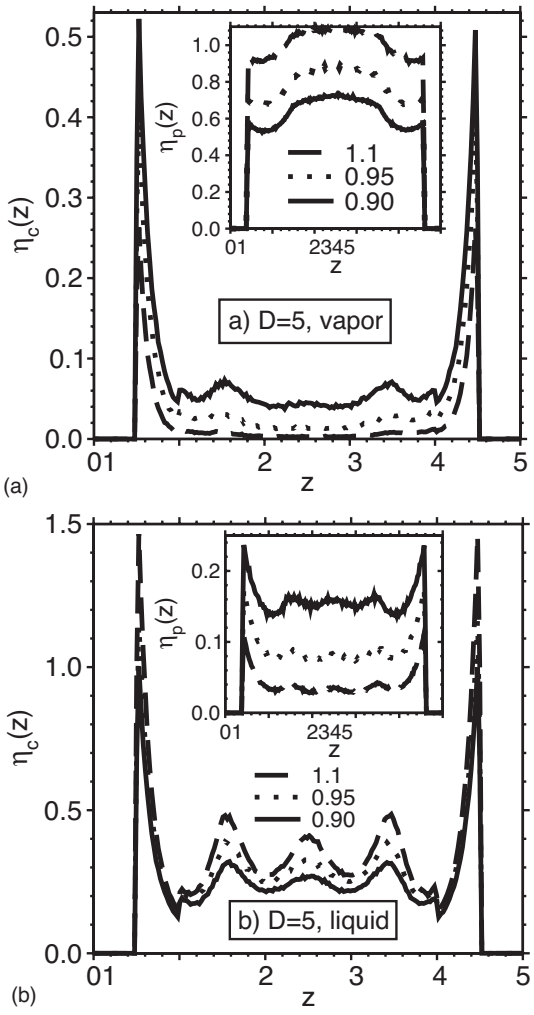

FIG. 9. Same as Fig. 8, but for $D=5$ and $L=20$.

scaling likely come into play. In view of this, the agreement of our data with the scaling predictions, Eqs. (2) and (3), is already rather satisfactory.

Finally, we consider the Kelvin equation, which is expected to describe the shift in the coexistence colloid chemical potential away from the critical point. It is expected that

$$(\Delta\mu)_{\text{Kelvin}} \equiv \mu_c^{\text{coex}}(D) - \mu_c^{\text{coex}}(\infty) \propto 1/D, \qquad (14)$$

with $\mu_c^{\text{coex}}(D)$ the coexistence chemical potential of the colloids in the confined system, and $\mu_c^{\text{coex}}(\infty)$ that in the bulk. Figure 7 presents a test of the Kelvin equation, plotting the chemical potential difference as function of D^{-1}, choosing three values of η_p^r which are much *higher* than the corresponding critical values $\eta_{p,\text{cr}}^r(D)$. Once again, some systematic deviations at very small thicknesses ($D=3$ and $D=5$) are seen, while for $D=7.5$ and $D=10$, one can already observe the expected straight lines through the origin.

D. Structural properties

We now consider the local structure in the thin films. Figures 8 and 9 show density profiles of colloids and polymers (the latter are shown as insets), as a function of the distance

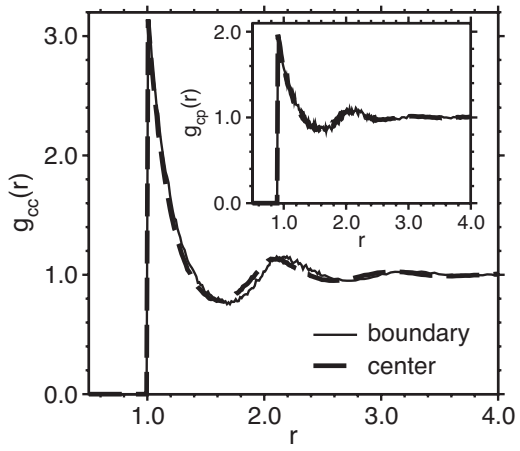

FIG. 10. Radial distribution functions $g_{cc}(r)$ (main frame) and $g_{cp}(r)$ (inset) obtained in planes *parallel* to the confining walls (see details in text) for a film with thickness $D=10$. The full curves show data obtained in the direct vicinity of the walls; the broken curves show data obtained in the bulk region of the film. Here, the bulk region was taken to be in the range $3.5 \leqslant z \leqslant 6.5$, where the corresponding density profile is essentially flat, see Fig. 8.

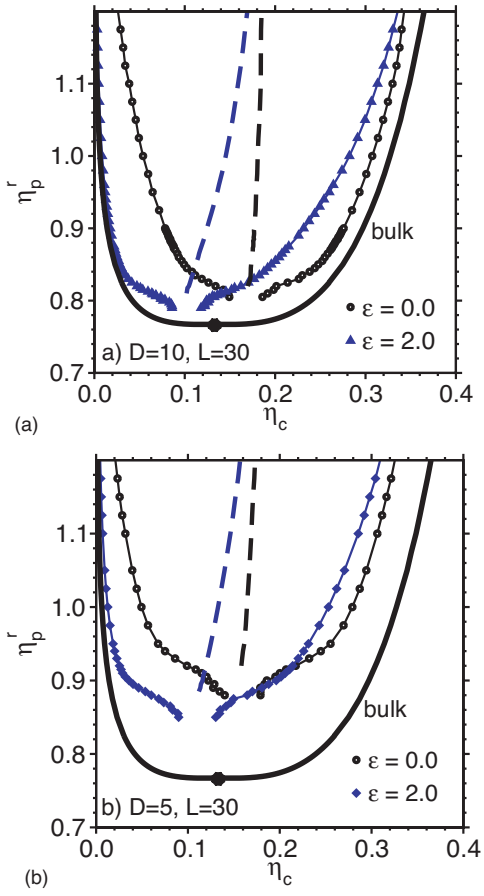

FIG. 11. (Color online) Binodal of the AO model with $q=0.8$ in bulk (full curve) and confinement (symbols). Shown are data for two system sizes $D=10$, $L=30$ (a) and $D=5$, $L=30$ (b). For each system size, two values of the colloid-wall interaction parameter ϵ, see Eq. (5), are considered. Broken lines indicate the coexistence diameters of the confined systems.

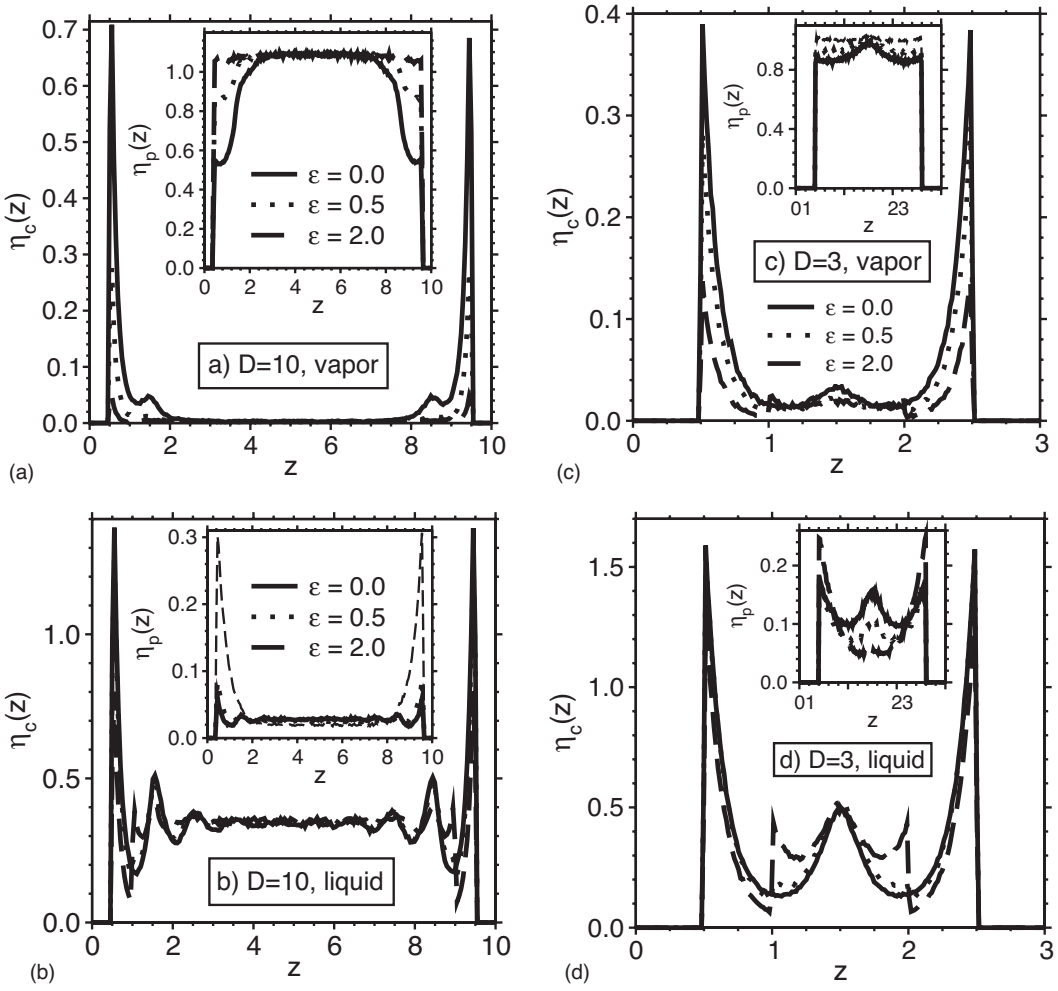

FIG. 12. Colloid density profiles obtained in thin films at $\eta_p^r=1.1$, for two values of the film thickness D, and several values of the colloid-wall parameter ϵ as indicated. Frames (a) and (b) show profiles obtained for $D=10$, on the vapor and liquid branch of the binodal, respectively. Frames (c) and (d) show the corresponding profiles for thickness $D=3$. The insets represent density profiles of the polymers.

z across the film. Results are shown for for $D=10$ (Fig. 8) and $D=5$ (Fig. 9). The three values of η_p^r are chosen well away from the critical point, such that finite size effects in L can safely be neglected. The upper panel in each figure shows profiles obtained in the colloidal "vapor" phase; the lower panel in the colloidal "liquid" phase, that coexists with the vapor. It is clear that, despite the repulsive colloid-wall energy [$\epsilon=0.5$ in Eq. (5)], the entropically driven attraction of the colloids to the walls still exists, and causes the formation of a rather dense layer of colloids at the walls. At not too large values of η_p^r, one can even see an indication of a second layer of colloids in the "vapor" phase. Of course, in the liquid phase, rather pronounced layering effects can always be detected. For the case $D=10$, there are three colloidal layers adjacent to each wall; in the range $3.5 \leqslant z \leqslant 6.5$, the density profiles are essentially horizontal. This flatness indicates bulklike behavior in the center of the thin film. In contrast, for the case $D=5$, the layering associated with the left wall "interferes" with layering effects at the right wall, and no bulk region can be identified. For the particular parameters considered here, Fig. 9 shows that only five layers of colloids can be accommodated in a slit $D=5$ colloid diameters wide. Note also the steplike increase in the colloid density at $z=1$ and $z=4$. This feature must be attributed to the step in the colloid-wall interaction, see Eq. (5).

In view of the high colloid density reached locally in the first layer adjacent to each wall, one may wonder whether this affects the lateral ordering of the colloids in planes parallel to the walls. Therefore, we have measured the radial distribution functions $g_{\alpha\beta}(r)$ for colloid-colloid pairs ($\alpha\beta=cc$) and colloid-polymer pairs ($\alpha\beta=cp$), on the liquid branch of the binodal. Here, r denotes the magnitude of the displacement vector $r=|\vec{r}_{ij}|$ between pairs of particles ($i,j=c,p$). We have determined $g_{\alpha\beta}(r)$ in the bulk region of the film (center), and in the vicinity of the walls, i.e., at a distance of 1σ from the walls. Note that, in a system with walls (or virtual boundaries that define, e.g., the center of the confined system), the definition of the radial distibution function is different from that in the bulk. In an isotropic system with periodic boundary conditions, $g_{\alpha\beta}(r)$ is normalized by a phase factor $4\pi r^2$. However, for the case that boundaries are present, this factor has to be modified such that it is then

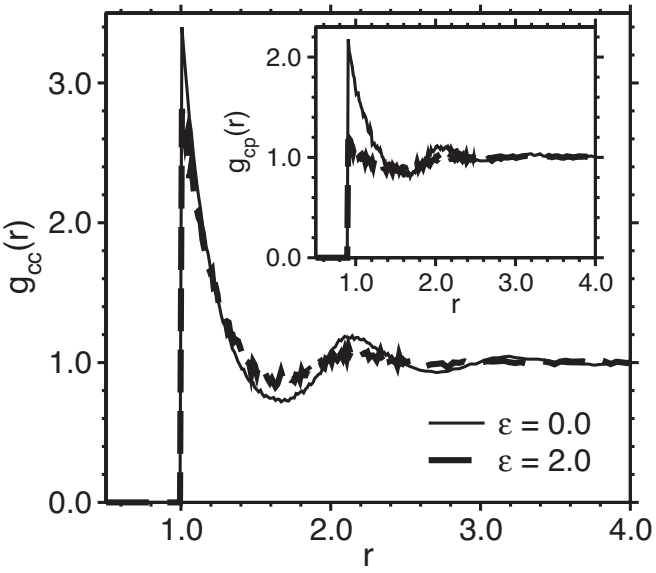

FIG. 13. Radial distribution functions $g_{cc}(r)$ (main frame) and $g_{cp}(r)$ (inset), obtained in the boundary layer adjacent directly to the walls, for two values of ϵ as indicated. Results were obtained for thickness $D=10$, $L=30$, and $\eta_p^r=1.1$.

determined only by that part of the surface $4\pi r^2$ of a sphere around a particle that fits into the system. Thus, the normalization factor depends on the distance of the particles from the walls in z direction. The result for $g_{\alpha\beta}(r)$ is illustrated in Fig. 10, for thickness $D=10$, lateral dimension $L=30$, and $\eta_p^r=1.1$. The important conclusion of Fig. 10 is that the radial distribution functions at the wall are almost indistinguishable from those of the bulk. This shows that, at the value of η_p^r considered here, there is still no sign of wall-induced crystallization. Corresponding data for other film thicknesses, $D=3$ and $D=5$, have also been collected, but show the same trend as in Fig. 10, and are therefore not shown.

V. INFLUENCE OF THE COLLOID-WALL INTERACTION

The results so far were obtained using $\epsilon=0.5$ in the colloid-wall interaction of Eq. (5). In this section, the parameter ϵ itself is varied, and the corresponding changes in the phase behavior (Fig. 11) and in the density profiles (Fig. 12) will be discussed. Figure 11 shows the binodal for thickness $D=10$ and $D=5$, for two different values of ϵ, compared to the bulk binodal. As before, $\epsilon=0$ implies pure hard walls [8]. We observe that, for large η_p^r, the binodal corresponding to $\epsilon=2.0$ and $D=10$, approaches the bulk binodal rather closely. This indicates that $\epsilon=2.0$ approximately cancels the entropic colloid-wall attraction. The latter is also evident from the corresponding density profiles, see Figs. 12(a) and 12(b). For $\epsilon=2.0$, the peak in the colloid density profile in the layers adjacent to the walls, is significantly reduced. In the liquid phase, we instead recognize a rather strong density jump for $\epsilon=2.0$, at both $z=1$ and $z=D-1$, due to the step in the colloid-wall potential. Only for $\epsilon=0$, do the density profiles remain smooth.

Clearly, in future work, a careful analysis of more realistic colloid-wall interactions is desirable. Such a study is moreover warranted because we find, see Fig. 13, that variations in ϵ significantly influence the radial distribution functions $g_{cc}(r)$ and $g_{cp}(r)$, measured at the walls. By increasing ϵ, a reduction of the first peak in $g_{cc}(r)$ occurs, with the second peak becoming almost completely washed out; for $g_{cp}(r)$ the effect is even more dramatic. As expected, increasing ϵ reduces the colloid density at the walls somewhat, thereby also weakening their tendency to order in the layers adjacent to the walls. Similar conclusions emerge from other wall thicknesses, too, and are therefore not shown here.

VI. DISCUSSION AND CONCLUDING REMARKS

Colloid-polymer mixtures are important model systems for the experimental exploration of fluid-fluid phase separation [19,20] and interfacial phenomena [21,22]. In order to guide possible future experiments on phase separation of such systems in confined geometry, we have carried out a simulation study of a generic model system, the AO model, confined to a slit formed by two parallel walls. The walls were not only impenetrable to both colloids and polymers, but in addition a short-ranged repulsive interaction between the walls and the colloids was added. Such an interaction can be realized, for instance, by a suitable coating of the walls with a moderately dense polymer brush (with the same chemical composition of the polymers dissolved in the solution). In this way, the strength of the depletion interaction between the colloid and the walls can be modified.

Our results show that the unmixing binodal, describing phase separation in colloid-polymer mixtures, changes dramatically from its bulk form, when the width of the pore is in the range of 3-10 colloid diameters. While such ultrathin pores seem to be experimentally realizable for colloidal systems, where the particle diameters are in the micrometer range, a corresponding study of a mixture of small molecules or atoms, clearly, would be extremely difficult, if not impossible. Surprisingly, even for thin pores, we find that bulklike phase behavior in the center of the pore is obtained, provided one is far away from criticality. Only for pores with thicknesses smaller than $D=3\sigma_c$ or so, can a bulklike region in the center of the pore no longer be identified. In this case, the layering induced in the density by the left wall interferes with the layering due to the right wall. Therefore, such extremely thin slit pores cannot be accounted for quantitatively in terms of a decomposition of their properties into bulk and surface properties. Hence, the description of the shift of the transition between the phases poor in colloids ("vapor") and rich in colloids ("liquid") in terms of the Kelvin equation, no longer is accurate. Nevertheless, agreement with the Kelvin equation is already recovered again above $D=10\sigma_c$ or so, which is still remarkably thin.

The main emphasis of this work, however, has been a study of the shift of the critical point. It has been shown that the scaling theory of Fisher and Nakanishi [5], originally formulated for the Ising lattice gas model exhibiting full particle-hole symmetry between the coexisting phases, is compatible with our present numerical results. A nontrivial

finding, which needs further investigation, is the fact that the critical value of the coexistence diameter approaches its limiting value in a nonmonotonic way when $D \to \infty$.

In our study, we have obtained not only accurate binodal curves of confined colloid-polymer mixtures, but we have also characterized the coexisting colloid-rich and colloid-poor phases in terms of their concentration profiles across the slit pore, and in terms of their radial distribution functions obtained in planes parallel to the walls. It would be interesting to extract corresponding information from experiments. Since the AO model is a crude simplification of reality, characteristic differences between simulation and experiment are to be expected, elucidating the limitations of the AO model.

In future work, we plan to extend our study to confinement between two parallel planar walls which are non-equivalent, whereby, for example, only one wall is coated by the polymer brush. In this way, an experimental realization of the interface localization-delocalization transition [4] may become possible. Also an extension of such studies to the dynamics of phase separation under confinement is of interest. We hope that the present work will stimulate corresponding experimental efforts.

ACKNOWLEDGMENTS

This work received financial support from the Deutsche Forschungsgemeinschaft (DFG) through the SFB-TR6, subprojects A5 and D3. Stimulating discussions with M. Dijkstra and H. N. W. Lekkerkerker are also acknowledged.

[1] D. E. Sullivan and M. M. Telo da Gama, in *Fluid Interfacial Phenomena*, edited by C. A. Croxton (Wiley, New York, 1985) p. 45.
[2] S. Dietrich, in *Phase Transitions and Critical Phenomena*, edited by C. Domb and J. L. Lebowitz (Academic Press, New York, 1988), Vol. 12, p. 1.
[3] M. Schick, in *Liquids at Interfaces*, edited by J. Charvolin, J.-F. Joanny, and J. Zinn-Justin (North-Holland, Amsterdam, 1990), p. 415.
[4] K. Binder, D. P. Landau, and M. Müller, J. Stat. Phys. **110**, 1411 (2003).
[5] M. E. Fisher and H. Nakanishi, J. Chem. Phys. **75**, 5857 (1981); H. Nakanishi and M. E. Fisher, *ibid.* **78**, 3279 (1983).
[6] R. Evans, J. Phys.: Condens. Matter **2**, 8989 (1990).
[7] L. D. Gelb, K. E. Gubbins, R. Radhakrishnan, and M. Sliwinska-Bartkowiak, Rep. Prog. Phys. **62**, 1573 (1999).
[8] R. L. C. Vink, K. Binder, and J. Horbach, Phys. Rev. E **73**, 056118 (2006).
[9] A more complete bibliography on the extensive literature on the subject can be found in Refs. [7,8].
[10] Y. Rouault, J. Baschnagel, and K. Binder, J. Stat. Phys. **80**, 1009 (1995).
[11] O. Dillmann, W. Janke, M. Müller, and K. Binder, J. Chem. Phys. **114**, 5853 (2001).
[12] F. Rouquerol, J. Rouquerol, and K. S. W. Sing, *Adsorption by Powders and Porous Solids: Principles, Methodology and Applications* (Academic Press, San Diego, 1999).
[13] *Nanoscale Science and Technology*, edited by R. Kelsall, I. W. Hamley, and M. Geoghegan (Wiley-VCH, Weinheim, 2005).
[14] T. M. Squires and S. R. Quake, Rev. Mod. Phys. **77**, 977 (2005).
[15] A. Patrykiejew, S. Sokolowski, and K. Binder, Surf. Sci. Rep. **37**, 207 (2000).
[16] W. C. Poon and P. N. Pusey, in *Observation, Prediction and Simulation of Phase Transitions in Complex Fluids*, edited by M. Baus, L. F. Rull, and J. P. Ryckaert (Kluwer Academic, Dordrecht, 1995), p. 3.
[17] A. K. Arora and B. V. R. Tata, Adv. Colloid Interface Sci. **78**, 49 (1998).
[18] H. Löwen, J. Phys.: Condens. Matter **13**, R415 (2001).
[19] W. C. Poon, J. Phys.: Condens. Matter **14**, R589 (2002).
[20] D. G. A. L. Aarts, J. H. van der Wiel, and H. N. W. Lekkerkerker, J. Phys.: Condens. Matter **15**, S245 (2003).
[21] D. G. A. L. Aarts, M. Schmidt, and H. N. W. Lekkerkerker, Science **304**, 847 (2004).
[22] D. G. A. L. Aarts and H. N. W. Lekkerkerker, J. Phys.: Condens. Matter **16**, S4231 (2004).
[23] S. Asakura and F. Oosawa, J. Chem. Phys. **22**, 1255 (1954).
[24] A. Vrij, Pure Appl. Chem. **48**, 471 (1976).
[25] M. Dijkstra and R. van Roij, Phys. Rev. Lett. **89**, 208303 (2002).
[26] M. Dijkstra and R. van Roij, J. Phys.: Condens. Matter **17**, S3507 (2005).
[27] M. Schmidt, A. Fortini, and M. Dijkstra, J. Phys.: Condens. Matter **15**, S3411 (2003); M. Schmidt, A. Fortini, and M. Dijkstra, *ibid.* **16**, S4159 (2004).
[28] A. Fortini, M. Schmidt, and M. Dijkstra, Phys. Rev. E **73**, 051502 (2006).
[29] R. L. C. Vink and J. Horbach, J. Chem. Phys. **121**, 3253 (2004); R. L. C. Vink, in *Computer Simulation Studies in Condensed Matter Physics XVII*, edited by D. P. Landau, S. P. Lewis, and H. B. Schüttler (Springer, Berlin, 2004).
[30] R. L. C. Vink and J. Horbach, J. Phys.: Condens. Matter **16**, S3807 (2004); R. L. C. Vink, J. Horbach, and K. Binder, J. Chem. Phys. **122**, 134905 (2005).
[31] M. E. Fisher, Rev. Mod. Phys. **46**, 587 (1974).
[32] M. E. Fisher and S.-Y. Zinn, J. Phys. A **26**, 201 (1998).
[33] J. Zinn-Justin, Phys. Rep. **344**, 159 (2001).
[34] K. Binder and E. Luijten, Phys. Rep. **344**, 179 (2001).
[35] R. J. Baxter, *Exactly Solved Models of Statistical Mechanics* (Academic Press, London, 1982).
[36] W. T. Thomson, Philos. Mag. **42**, 448 (1871).
[37] K. Binder and P. C. Hohenberg, Phys. Rev. B **6**, 3461 (1972); **9**, 2194 (1974).
[38] K. Binder, in *Phase Transitions and Critical Phenomena*, edited by C. Domb and J. L. Lebowitz (Academic Press, London, 1983), Vol. 8, p. 1.
[39] K. Binder and D. P. Landau, Phys. Rev. Lett. **52**, 318 (1984); D. P. Landau and K. Binder, Phys. Rev. B **41**, 4633 (1990).
[40] C. Ruge, S. Dunkelmann, F. Wagner, and J. Wulf, J. Stat. Phys.

73, 293 (1993); C. Ruge and F. Wagner, Phys. Rev. B **52**, 4209 (1995).
[41] H. W. Diehl and M. Shpot, Nucl. Phys. B **528**, 595 (1998).
[42] N. B. Wilding, in *Annual Reviews of Computational Physics*, edited by D. Stauffer (World Scientific, Singapore, 1996) p. 37.
[43] I. Brovchenko, A. Geiger, and A. Oleinikova, Phys. Chem. Chem. Phys. **3**, 1567 (2001); J. Phys.: Condens. Matter **16**, S5345 (2004).
[44] I. Brovchenko, A. Geiger, and A. Oleinikova, Eur. Phys. J. B **44**, 345 (2005); A. Oleinikova, I. Brovchenko, and A. Geiger, J. Phys.: Condens. Matter **17**, 7845 (2005).
[45] A. Oleinikova, I. Brovchenko, and A. Geiger, Eur. Phys. J. (to be published).
[46] P. G. de Gennes, *Scaling Concepts in Polymer Physics* (Cornell University Press, Ithaca, NY, 1979).
[47] P. Virnau and M. Müller, J. Chem. Phys. **120**, 10925 (2004).
[48] K. Binder and D. P. Landau, Phys. Rev. B **30**, 1477 (1984).
[49] C. Borgs and S. Kappler, Phys. Lett. A **171**, 37 (1992); C. Borgs and R. Kotecky, J. Stat. Phys. **61**, 79 (1990).
[50] K. Binder and D. W. Heermann, *Monte Carlo Simulation in Statistical Physics: An Introduction*, 4th ed. (Springer, Berlin, 2002).
[51] D. P. Landau and K. Binder, *A Guide to Monte Carlo Simulation in Statistical Physics*, 2nd ed. (Cambridge University Press, Cambridge, 2005).
[52] K. Binder, Z. Phys. B: Condens. Matter **43**, 119 (1981).
[53] Y. C. Kim, M. E. Fisher, and E. Luijten, Phys. Rev. Lett. **91**, 065701 (2003); Y. C. Kim and M. E. Fisher, Comput. Phys. Commun. **169**, 295 (2005); Y. C. Kim, Phys. Rev. E **71**, 051501 (2005).
[54] G. Kameniarz and H. W. J. Blöte, J. Phys. A **26**, 201 (1993).
[55] Y. C. Kim, M. E. Fisher, and G. Orkoulas, Phys. Rev. E **67**, 061506 (2003).
[56] A. Anisimov (private communication); R. L. C. Vink and H. H. Wensink, Phys. Rev. E **74**, 010102(R) (2006).